Research article

Lower complexity of motor primitives ensures robust control of high-speed human locomotion

Alessandro Santuz [a,b,*], Antonis Ekizos [a,b], Yoko Kunimasa [c], Kota Kijima [c], Masaki Ishikawa [c], Adamantios Arampatzis [a,b]

[a] Department of Training and Movement Sciences, Humboldt-Universität zu Berlin, 10115 Berlin, Germany
[b] Berlin School of Movement Science, Humboldt-Universität zu Berlin, 10115 Berlin, Germany
[c] Graduate School of Sport and Exercise Sciences, Osaka University of Health and Sport Sciences, 590-0459 Osaka, Japan

ARTICLE INFO

ABSTRACT

Walking and running are mechanically and energetically different locomotion modes. For selecting one or another, speed is a parameter of paramount importance. Yet, both are likely controlled by similar low-dimensional neuronal networks that reflect in patterned muscle activations called muscle synergies. Here, we challenged human locomotion by having our participants walk and run at a very broad spectrum of submaximal and maximal speeds. The synergistic activations of lower limb locomotor muscles were obtained through decomposition of electromyographic data via non-negative matrix factorization. We analyzed the duration and complexity (via fractal analysis) over time of motor primitives, the temporal components of muscle synergies. We found that the motor control of high-speed locomotion was so challenging that the neuromotor system was forced to produce wider and less complex muscle activation patterns. The motor modules, or time-independent co-efficients, were redistributed as locomotion speed changed. These outcomes show that humans cope with the challenges of high-speed locomotion by adapting the neuromotor dynamics through a set of strategies that allow for efficient creation and control of locomotion.

1. Introduction

Humans can locomote at a very broad range of speeds even though walking and running, the two most common gait modes, are profoundly different from both a mechanic and energetic point of view [1, 2, 3]. Walking, with its characteristic double support stance phase, typically implies at least one limb being in contact with the ground, while running allows for a flight phase [4]. Moreover, the energy cost function of walking has a peculiar U-shape with a minimum close to each individual's preferred speed, which lies around 1.4 m/s in the average human [5]. At lower and higher speeds, walking is relatively costlier but remains more economical than running until circa 2.4 m/s, speed at which running becomes more economical than walking [1, 5]. Humans often decide to switch from walking to running at lower speeds [5], on average around 2.0 m/s. The cost of running is quasi-linearly correlated with

speed, at least if the nonlinear contribution of air resistance is neglected [5, 6, 7]. Yet, despite the profound mechanical and energetic differences, walking and running seem to be sharing similar neural control [4, 8, 9].

The exceptional amount of degrees of freedom available to vertebrates for accomplishing any kind of movement is defined by the vast number of muscles and joints [10]. Nevertheless, the central nervous system manages to overcome complexity, possibly through the orchestrated activation of functionally-related muscle groups, rather than through muscle-specific commands [10, 11]. The generation of rhythmic and patterned activity such as that needed for locomotion is achieved through neuronal networks located in the spinal cord that do not require sensory input to work: the central pattern generators [12, 13, 14, 15]. However, these circuits need supraspinal input to modulate basic locomotor functions, such as gait type selection, speed control and perturbation management [16, 17]. The finely coordinated motor output is

* Corresponding author.
E-mail address: alessandro.santuz@hu-berlin.de (A. Santuz).

achieved by interconnecting the central pattern generators and the drive from higher centers with integration of sensory feedback information [10, 18, 19, 20, 21, 22, 23, 24, 25], ultimately resulting in accurate activation patterns. Using computational approaches, it has been previously shown that these patterns, called muscle synergies, are common to different muscles and are task-specific [26]. Usually extracted from electromyographic (EMG) data via linear machine learning approaches such as the non-negative matrix factorization (NMF), muscle synergies have been increasingly employed in the past two decades for providing indirect evidence of a simplified, modular control of movement in humans and other vertebrates [27, 28, 29, 30, 31].

In this study, we extracted muscle synergies from the EMG activities of lower limbs during treadmill walking and running at several speeds, from slow walking to maximal sprinting. Synergies were divided into time-independent (motor modules) and time-dependent (motor primitives) coefficients. The Higuchi's fractal dimension (HFD) was used to evaluate the local complexity of motor primitives, taken as self-affine time series [9, 32, 33, 34, 35]. Defining robustness as the ability to cope with perturbations [8], it follows that biological systems can manage to maintain function despite disturbances only through robust control [36, 37, 38]. Assessing the complexity of control signals could give us an idea of the strategies adopted by the central nervous system to cope with disruptions. Recently, we showed that challenging locomotion
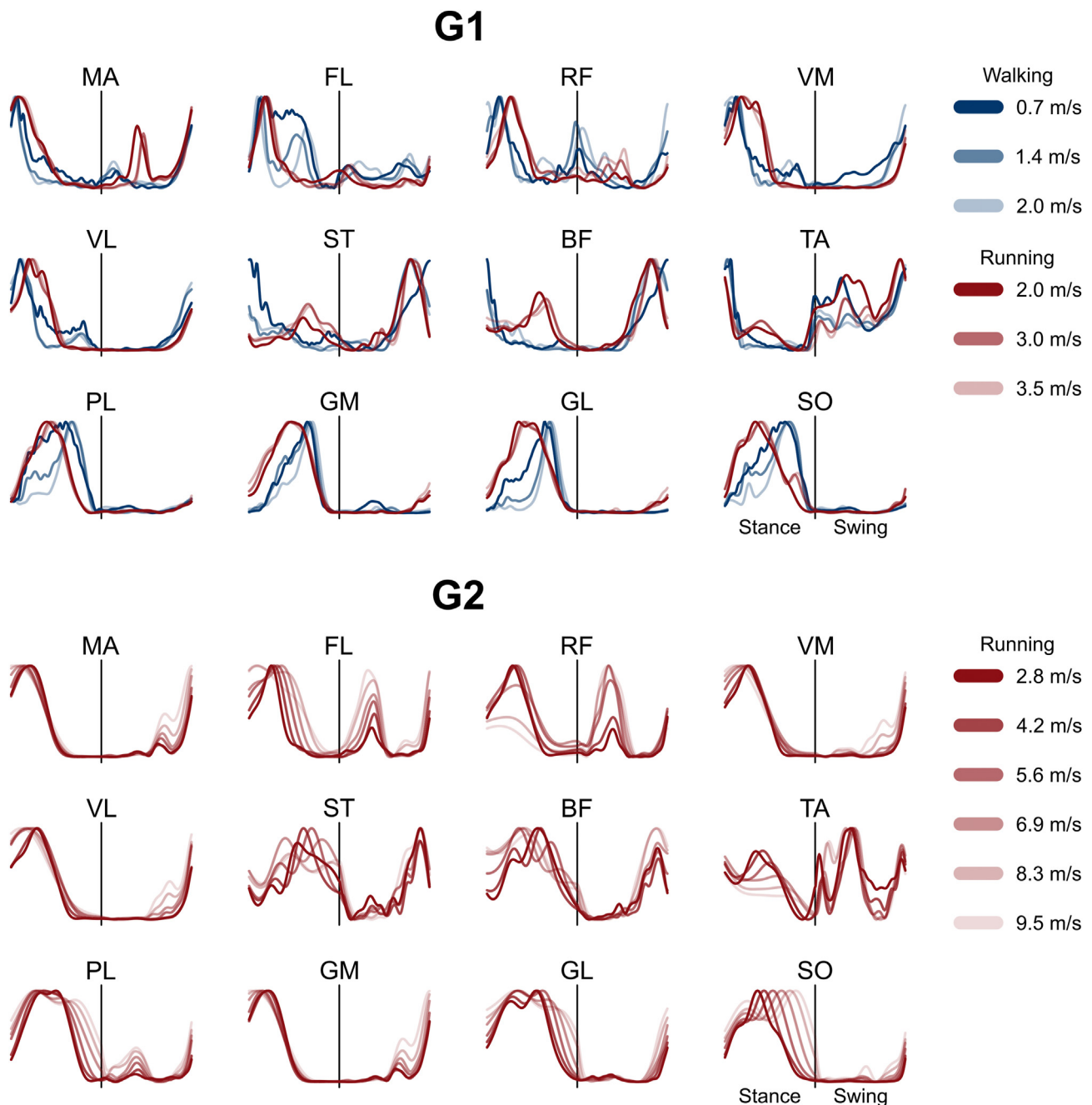

Figure 1. Average electromyographic activity of lower limb muscles. Average EMG activity of the recorded muscles at different speeds in group 1 (G1) and group 2 (G2). The x-axis full scale represents the averaged gait cycle (with stance and swing normalized to the same amount of points and divided by a vertical line) and the y-axis the amplitude normalized to the maximum. Muscle abbreviations: MA = *gluteus maximus*, FL = *tensor fasciæ latæ*, RF = *rectus femoris*, VM = *vastus medialis*, VL = *vastus lateralis*, ST = *semitendinosus*, BF = *biceps femoris*, TA = *tibialis anterior*, PL = *peroneus longus*, GM = *gastrocnemius medialis*, GL = *gastrocnemius lateralis*, SO = *soleus*.

conditions (i.e., in the presence of external mechanical perturbations and in aging) manifest lowered complexity of motor primitives [9]. Moreover, we and others proposed that the width of motor primitives increases to ensure robust control in the presence of internal and external perturbations [8, 31, 39, 40, 41], suggesting that this might be a compensatory mechanism adopted by the neuromotor system to cope with the postural instability of locomotion in health and pathology [39, 40]. We observed the neural strategy of motor primitive widening in wild-type mice [31] and in humans affected by multiple sclerosis [42] or healthy adults undergoing external perturbations [8, 9], but not in genetically modified mice that lacked feedback from proprioceptors [31]. Due to these observations, we concluded that intact systems use relatively wider (i.e., of relatively longer duration) and less complex control signals to regulate motor function through robust control [8, 9, 42].

Here, we used the challenges imposed by slow and increasingly high speeds to perturb the locomotor system. We hypothesized that forcing the central nervous system to control increasingly higher speeds would perturb the system to the point of eliciting an increased control's robustness. We discovered that motor primitives become wider and less complex as locomotion speed increases, translating into robust control. Moreover, we found that walking and running shared similar motor modules that were regulated depending on speed, confirming previous

results obtained by other authors [4, 43, 44, 45, 46]. These findings provide further insight into the neuromotor dynamics of challenging locomotion. A topic with broad implications in human pathology and performance, robotics, comparative biology and other locomotion-related fields.

2. Results

2.1. Muscle synergies

The EMG activities from which muscle synergies were extracted are presented in Figure 1 as average of all trials. The average number of synergies which best accounted for the EMG data variance (i.e., the factorization rank) of G1 was 4.3 ± 0.6 (walking, 0.7 m/s), 4.4 ± 0.5 (walking, 1.4 m/s), 4.3 ± 0.5 (walking, 2.0 m/s), 4.1 ± 0.4 (running, 2.0 m/s), 4.3 ± 0.7 (running, 3.0 m/s), and 4.3 ± 0.6 (running, 3.5 m/s). In G2, the values were 4.1 ± 0.5 (running, 2.8 m/s), 3.9 ± 0.6 (running, 4.2 m/s), 3.9 ± 0.5 (running, 5.6 m/s), 3.9 ± 0.5 (running, 6.9 m/s), 4.0 ± 0.0 (running, 8.3 m/s), and 4.2 ± 0.4 (running, 9.5 m/s). We did not find a significant effect of speed on the factorization rank ($p = 0.797$ for G1, $p = 0.320$ for G2).

The functional classification (see methods) identified four fundamental muscle synergies in both groups (Figures 2 and 3). The first
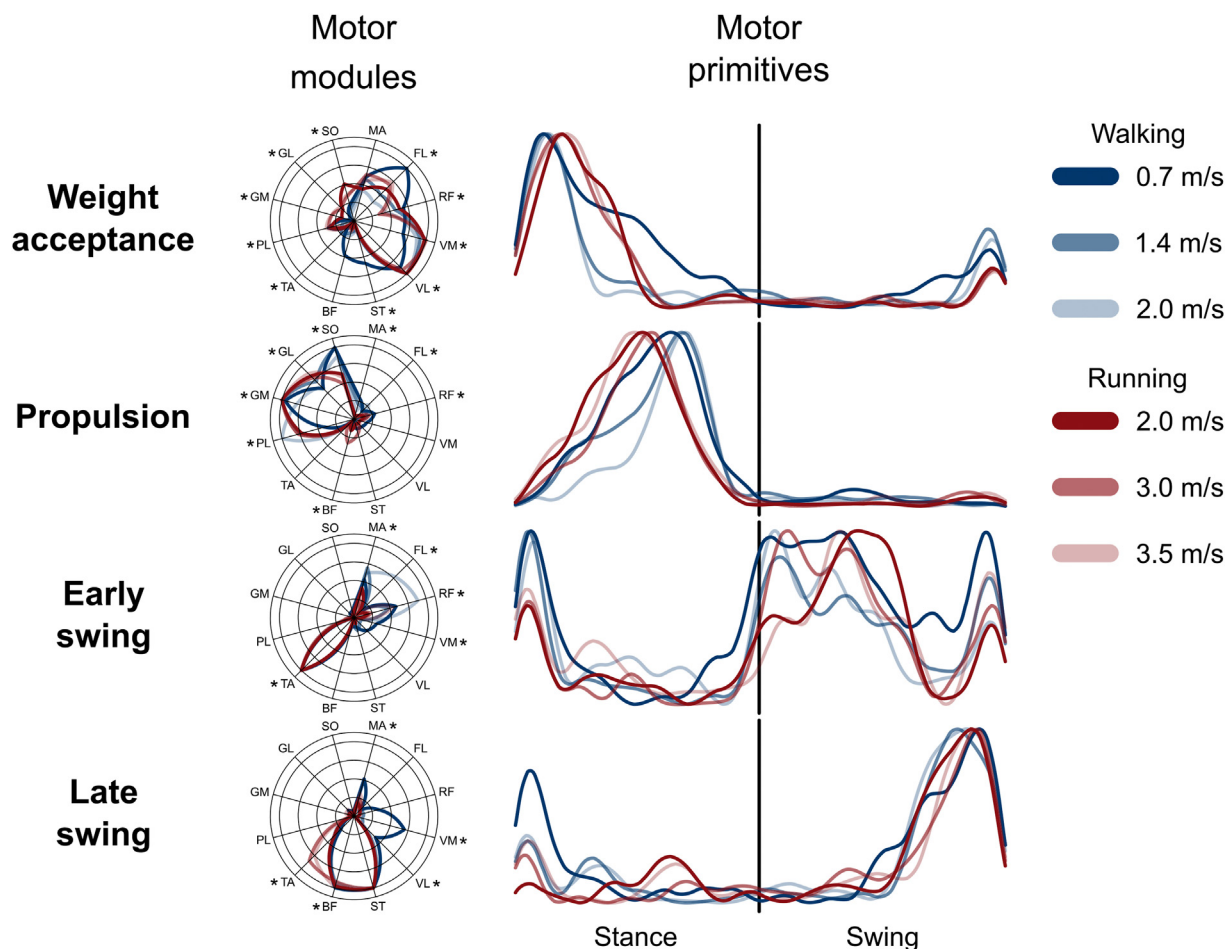

Figure 2. Muscle synergies for human walking and running at various speeds. Motor modules and motor primitives of the four fundamental synergies for human walking and submaximal running (average of all trials recorded in group 1). The motor modules are presented in polar coordinates on a normalized polar axis base. Each muscle contribution within one synergy can range from 0 to 1 (maximum radius length). Asterisks represent significant effect of speed (results of the *post-hoc* analysis, where relevant). For the motor primitives, the x-axis full scale represents the averaged gait cycle (with stance and swing normalized to the same amount of points and divided by a vertical line) and the y-axis the normalized amplitude. Muscle abbreviations: MA = *gluteus maximus*, FL = *tensor fasciæ latæ*, RF = *rectus femoris*, VM = *vastus medialis*, VL = *vastus lateralis*, ST = *semitendinosus*, BF = *biceps femoris*, TA = *tibialis anterior*, PL = *peroneus longus*, GM = *gastrocnemius medialis*, GL = *gastrocnemius lateralis*, SO = *soleus*.
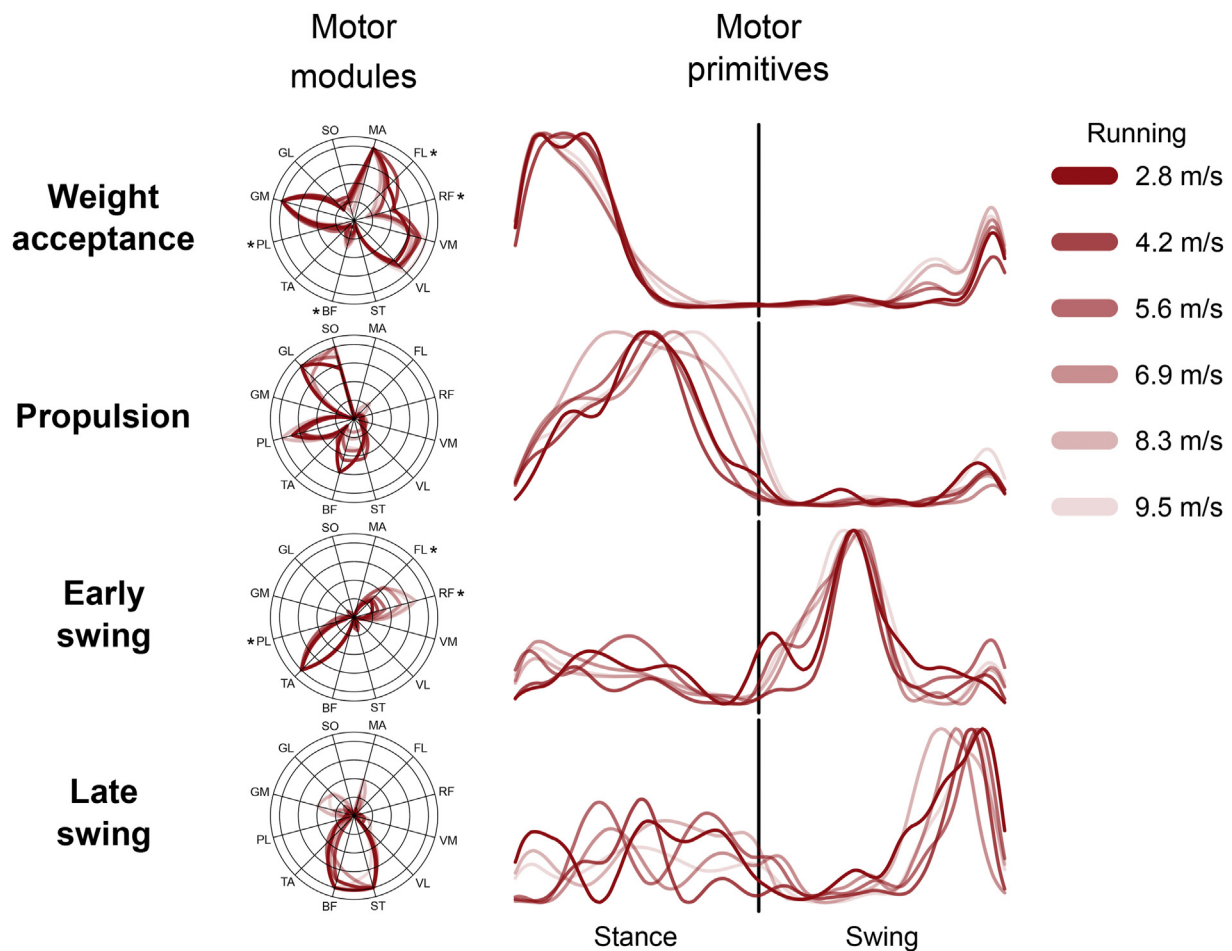
Figure 3. Muscle synergies for human running at various speeds. Motor modules and motor primitives of the four fundamental synergies for human submaximal and maximal running (average of all trials recorded in group 2). The motor modules are presented in polar coordinates on a normalized polar axis base. Each muscle contribution within one synergy can range from 0 to 1 (maximum radius length). Asterisks represent significant effect of speed (results of the *post-hoc* analysis, where relevant). For the motor primitives, the x-axis full scale represents the averaged gait cycle (with stance and swing normalized to the same amount of points and divided by a vertical line) and the y-axis the normalized amplitude. Muscle abbreviations: MA = *gluteus maximus*, FL = *tensor fasciæ latæ*, RF = *rectus femoris*, VM = *vastus medialis*, VL = *vastus lateralis*, ST = *semitendinosus*, BF = *biceps femoris*, TA = *tibialis anterior*, PL = *peroneus longus*, GM = *gastrocnemius medialis*, GL = *gastrocnemius lateralis*, SO = *soleus*.

synergy functionally referred to the body weight acceptance, with a major involvement of knee and hip extensors. The second synergy was associated with the propulsion phase, to which the ankle plantarflexors mainly contributed. The third synergy identified the early swing and

showed the involvement of ankle dorsiflexors and, at high locomotion speeds in both walking and running, of hip flexors. The fourth and last synergy reflected the late swing and the landing preparation, highlighting the relevant influence of knee flexors and ankle dorsiflexors. As

Table 1. Frequency of occurrence of fundamental synergies. Even though the factorization rank was not influenced by locomotion speed, not all the extracted synergies could be functionally classified as fundamental (i.e., not combined). This table reports the number of participants that showed the relevant fundamental synergies at each speed for both groups (G1 = walking and submaximal running, G2 = submaximal and maximal running).

Group	Speed [m/s]		Synergy			
			Weight acceptance	Propulsion	Early swing	Late swing
G1 (15 participants)	Walking	0.7	10	15	13	6
		1.4	13	15	9	15
		2.0	13	15	7	15
	Running	2.0	15	15	6	11
		3.0	15	14	2	14
		3.5	15	15	3	12
G2 (15 participants)	Running	2.8	15	13	8	4
		4.2	15	15	5	1
		5.6	15	15	11	4
		6.9	15	14	9	1
		8.3	15	12	14	2
		9.5	15	9	15	5

showed in the past for other locomotion conditions [8, 47, 48, 49, 50], not all the participants exhibited all the four fundamental synergies at all speeds; in particular, 27% and 30% of the total synergies were classified as combined in walking and running, respectively. We reported the

detailed numbers in Approximate position of Table 1. The effect of speed on motor modules is reported in Figures 2 and 3, where asterisks denote the outcome of the *post-hoc* analysis.
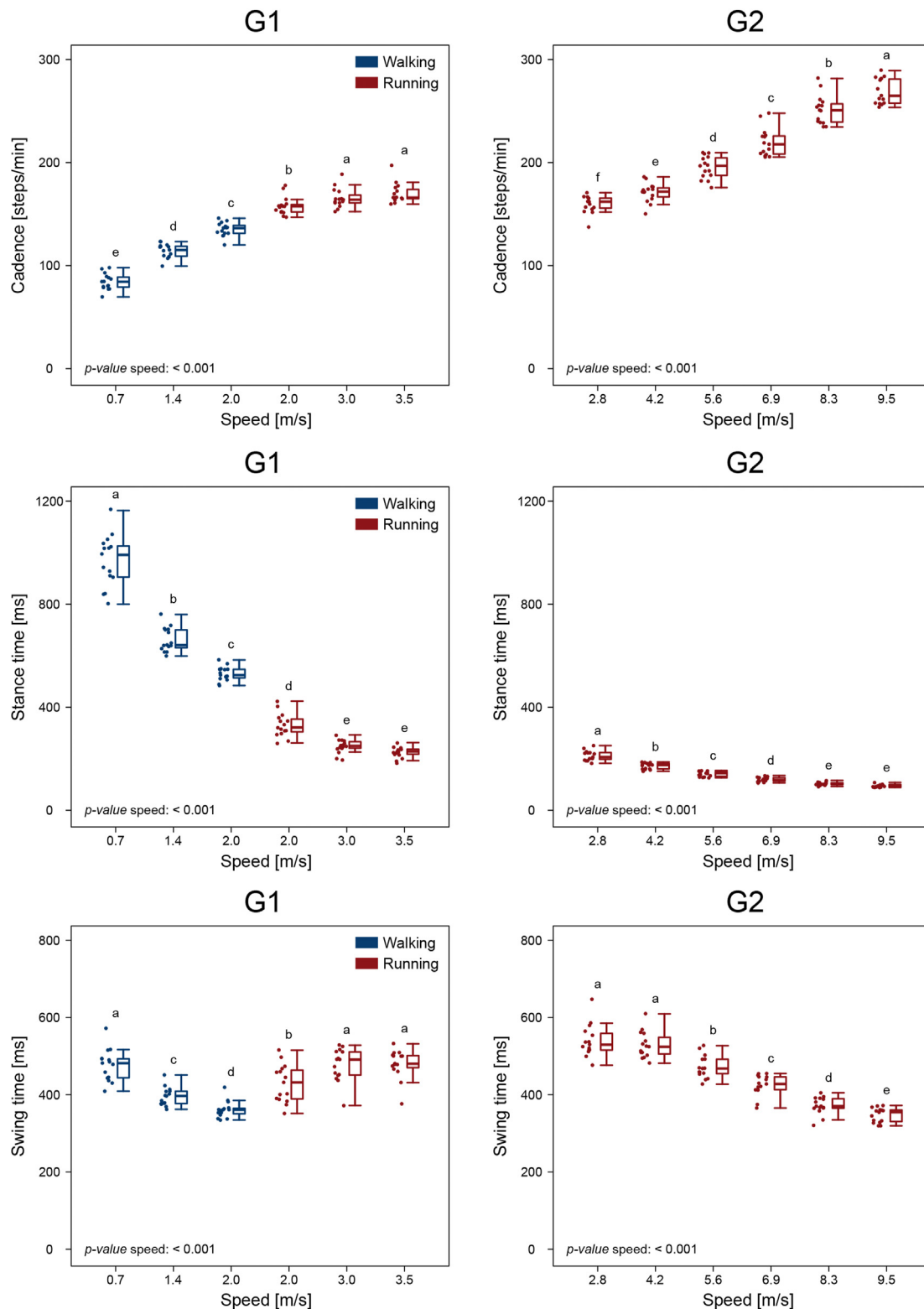

Figure 4. Gait cycle spatiotemporal parameters. Boxplots describing the cadence (in steps per minute), stance and swing times for the two groups (G1 = walking and submaximal running, G2 = submaximal and maximal running). Boxplots sharing the same letter (a, b, c, d, e) are not to be considered significantly different (results of the *post-hoc* analysis). Raw data points are presented to the left side of each boxplot. "*p-value* speed: < 0.001": when a given parameter presents a significant speed effect (p < 0.001).

2.2. Gait cycle parameters

An effect of speed (p < 0.001) was found in both groups for the cadence and the swing and stance times (Figure 4). When locomotion speed increased, cadence increased as well, while stance times decreased. In walking (G1), swing times decreased with increasing speed. In running (G1), swing times increased between 2.0 and 3.0 m/s, but were not significantly different at 3.0 and 3.5 m/s. In G2, swing times decreased with increasing speed after 4.2 m/s. The strike index during running was, in G1, of 0.23 ± 0.26 at 2.0 m/s, 0.22 ± 0.25 at 3.0 m/s and 0.24 ± 0.26 at 3.5 m/s, all indicating a rearfoot strike pattern. In G2, the strike index values during running were 0.50 ± 0.18 at 2.8 m/s, 0.57 ± 0.13 at 4.2 m/s, 0.62 ± 0.11 at 5.6 m/s, 0.65 ± 0.11 at 6.9 m/s, 0.70 ± 0.10 at 8.3 m/s and 0.74 ± 0.06 at 9.5 m/s, all indicating a mid/forefoot strike pattern.

2.3. Higuchi's fractal dimension of motor primitives

The HFD of motor primitives is reported in Approximate position of Figure 5. In both groups, the HFD was affected by speed (p < 0.001), with a global tendency towards a lower complexity (i.e., lower HFD) of motor primitives with increasing speed. Specifically, in G1 the highest complexity was found in walking at 0.7 m/s, with values decreasing significantly as the speed increased to 1.4 m/s and until 2.0 m/s; running faster from 2.0 to 3.0 m/s induced decreased HFD (Approximate position of Figure 5). In G2, the complexity in essence decreased with speed until 9.5 m/s, although with no significant difference between 4.2 and 5.6 m/s, 6.9 and 8.3 m/s, and 8.3 and 9.5 m/s (Approximate position of Figure 5).

2.4. Width of motor primitives

The width of motor primitives, measured with the FWHM, was significantly affected by speed only for the primitives of the stance synergies (i.e., weight acceptance and propulsion) in both G1 and G2 (p < 0.001). The boxplots depicting the changes in FWHM with speed are shown in Approximate position of Figure 6. In G1, the weight acceptance and propulsion primitives were wider in running than in walking, but speed played little if any role within the same locomotion type. In G2 there was a widening of the weight acceptance synergies after 5.6 m/s, while the propulsion synergies became wider with increasing speed at almost all speeds. The primitives of the early and late swing synergies did not show any change attributable to the different locomotion speed

(early swing, G1: p = 0.133; late swing, G1: p = 0.029, *post-hoc* analysis did not confirm an effect of speed; early swing, G2: p = 0.385; late swing, G2: p = 0.391).

3. Discussion

In this study, we used a broad range of gait speeds to differentially challenge the human locomotor system. Our analysis of the modular organization of muscle activations in adult males showed that increasing the locomotion speed and transitioning from walking to running forced the motor system to produce locally less complex (i.e., lower HFD) and relatively longer (i.e., higher FWHM) basic activation patterns (i.e., motor primitives). Moreover, in both walking and running, we found a speed-dependent redistribution of muscle contributions (i.e., motor modules) within the muscle synergies. While not generalizable to the female population due to the male sample, these findings provide evidence that the neuromotor control of locomotion via muscle synergies was spatially and temporally modulated to withstand the constraints imposed by high locomotion speeds.

Recently, we used the HFD, a nonlinear measure of local complexity derived from fractal analysis [32], to show that the motor primitives extracted from challenging locomotion conditions exhibit lower complexity than those associated with normal locomotion [9]. Specifically, we showed that older age and external perturbations induce the locomotor system to lower the complexity of motor primitives [9]. In this study, we found a similar behavior depending on the speed at which our participants were walking or running. From the slowest (walking at 0.7 m/s) to the fastest speed (sprinting at 9.5 m/s), complexity of motor primitives decreased rather smoothly. In addition, primitives proved to be locally less complex in running than in walking, relative to the time-normalized gait cycle. This decrease in complexity can be interpreted as a strategy adopted by the central nervous system to robustly cope with the challenges imposed by high locomotion speeds. In fact, running allows less time for organizing coordinated movements than walking [51] and a simplification of control could benefit its robustness. Similarly, one could explain the need for lower complexity of motor primitives when locomotion speeds approach those of sprinting, with stance times well below 150 ms, swing times of less than 400 ms and cadence exceeding 250 steps per minute.

Lower complexity indicates lower nonlinearity of the physiological signal [52]. In this study, we considered motor primitives as the basic neuromotor entities for the control of walking and running over time. It
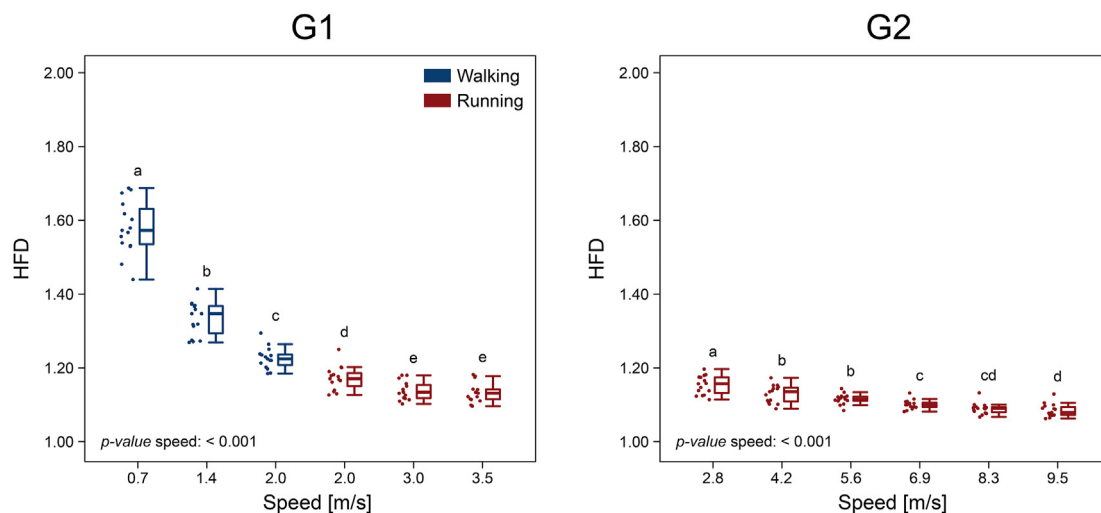

Figure 5. Higuchi's fractal dimension of motor primitives. Boxplots describing the Higuchi's fractal dimension (HFD) of the motor primitives extracted from the two groups (G1 = walking and submaximal running, G2 = submaximal and maximal running). Boxplots sharing the same letter (a, b, c, d, e) are not to be considered significantly different (results of the *post-hoc* analysis). Raw data points are presented to the left side of each boxplot. "*p-value* speed: < 0.001": when a given parameter presents a significant speed effect (p < 0.001).

has been shown that the complexity of electroencephalographic activity is reduced by degeneration and dysfunction of neural networks, e.g., due to aging, neurodegenerative diseases, brain injury and stroke [52]. Associated to our previous finding of a decreased complexity of locomotor primitives with aging and external perturbations [9], it is tempting to link decreased neuromotor complexity with internally- or externally-imposed constraints to movement. From a neurophysiological perspective, this could represent a strategy used by vertebrates to create and control efficient locomotion despite system-related or environmental disturbances. Under this hypothesis, the ability to modulate complexity might in fact be a determinant of sprinting performance and/or response to training or rehabilitation. Based on the present findings, we suggest that interventions focused on the regulation of motor primitive complexity could be used to assess and possibly improve the performance of high-speed locomotion (walking and running). This idea might pave the way for the establishment of future training intervention protocols based on walking and running and aimed not only at athletes but possibly

also at specific groups of patients suffering from neurological diseases or recovering from injury.

Furthermore, we found a relative widening of motor primitives in the two synergies relevant for the stance phase (i.e., the weight acceptance and propulsion synergies) at increasing locomotion speeds. This observation seems to confirm previous findings that more challenging locomotion conditions (in this case maximal as compared to submaximal running or fast as compared to slow walking) demand more robust motor control achieved by widening the primitives of the stance phase [8, 9]. Recently we found that, in the presence of perturbations, the central nervous system of both humans and mice generates wider basic activation patterns of muscle groups, which makes the motor execution less prone to the influence of external perturbations [8, 9, 31, 42, 53]. We concluded that wider (i.e., active for a relatively longer period of time) primitives indicate more robust control [8, 9, 31, 42, 53]. The overlap of chronologically-adjacent synergies increased the fuzziness [37, 42, 54] of temporal boundaries allowing for easier shifts between one synergy (or gait phase) and another when perturbations were added to locomotion
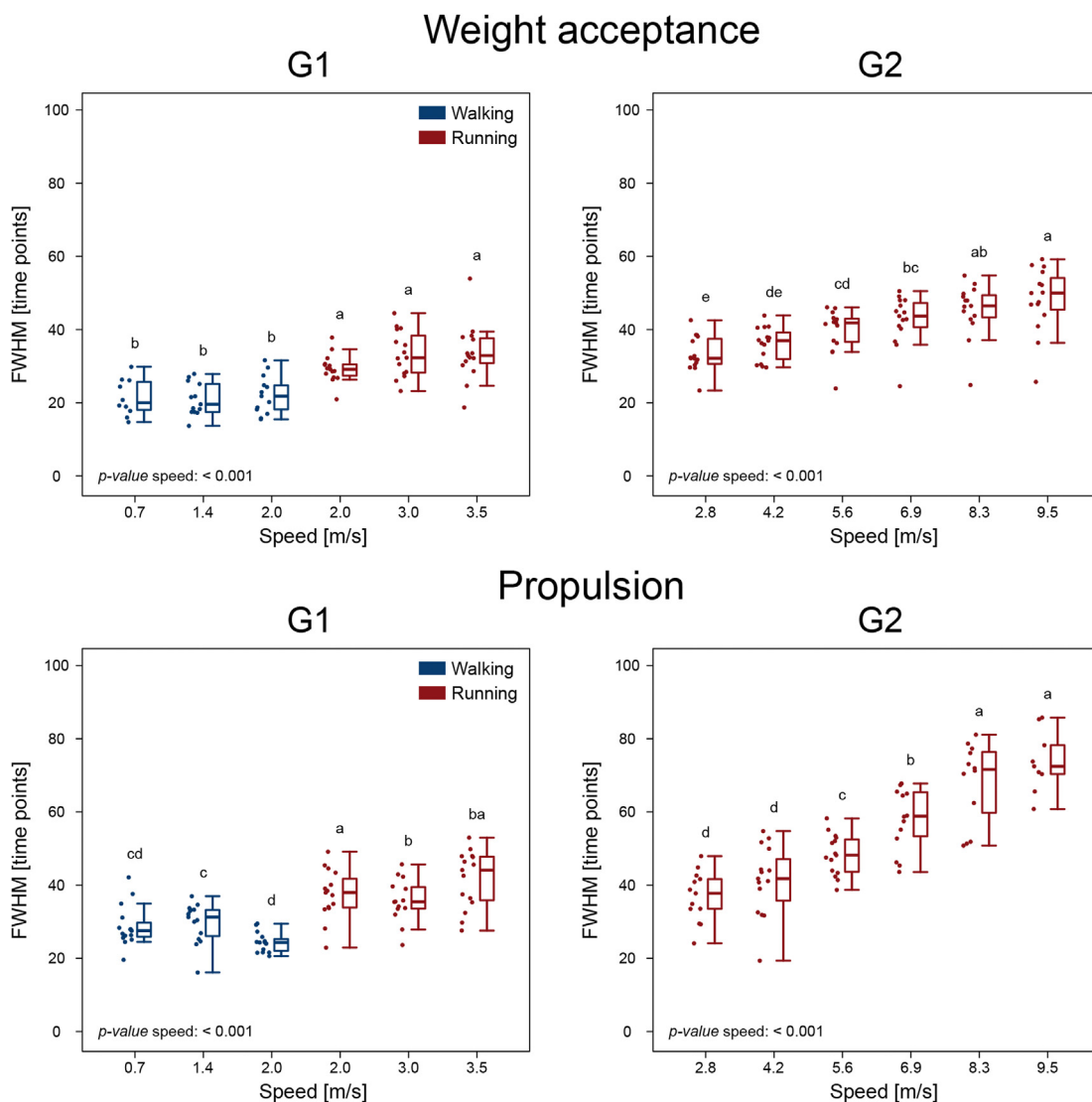

Figure 6. Width of motor primitives. Boxplots showing the width of motor primitives measured with the full width at half maximum (FWHM) in normalized time points for the two groups (G1 = walking and submaximal running, G2 = submaximal and maximal running). Only the primitives that showed significant effect of speed on the FWHM are showed (i.e., the motor primitives relative to the weight acceptance and propulsion synergies; the early and late swing synergies did not show any significant effect of speed on the FWHM of motor primitives). Boxplots sharing the same letter (a, b, c, d, e) are not to be considered significantly different (results of the *post-hoc* analysis). Raw data points are presented to the left side of each boxplot. "*p-value* speed: < 0.001": when a given parameter presents a significant speed effect (p < 0.001).

[8, 9, 31, 42, 53]. Our conclusion fits the optimal feedback control theory, which postulates that motor systems selectively use feedback information to optimize an index of performance by combining sensory signals and motor commands [55, 56, 57]. For the central nervous system, this solution must come at the cost of reducing the accuracy or, as others called it, optimality [37] or efficiency [58].

The relative FWHM increased not only with running speed, but also when switching from walking to running. One possible reason could lie in the fact that the motor primitives for the two locomotion types have different shapes in the weight acceptance and propulsion synergy. Specifically, walking primitives are skewed to the left in the weight acceptance and to the right in the propulsion phase, while running primitives appear symmetrical. In walking, the leading leg has a bigger angle at touchdown than in running and this determines the position of the body's center of mass [59]. This physically constrains the production of forward forces in walking from the plantarflexors [8, 60, 61, 62, 63, 64], since only after half stance there can be propulsion, while in running it can happen earlier [2]. Nonetheless, our outcomes confirm the notion [28, 65] that, in both walking and running, motor primitives are shaped in a way that ensures the adequate duration of activation at each speed (i.e., shorter at higher speeds, longer at slower speeds), even though this modulation was present only in the stance phase and in different amounts when comparing the weight acceptance and the propulsion primitives.

The question remains as to why HFD values were lower when the walking or running speed increased and in walking compared to running. Due to its definition (Eq. 4), the HFD depends on the signal-to-noise ratio [66], but some precautions can be taken to reduce the influence of the signal-to-noise ratio on the outcomes (i.e., minimum subtraction and normalization to the maximum). Nevertheless, due to the summation term in Eq. (4), which represents the absolute value of the successive differences of each motor primitive's ordinates, calculated with lag k (see methods), curves with relatively greater FWHM will have a lower $L(k)$. From a physiological point of view this could mean that the central nervous system deals with the challenge of controlling locomotion at high speeds by increasing the relative FWHM of control signals, a solution that results in locally less complex motor primitives (i.e., lower HFD) relative to the time-normalized gait cycle. Yet, the increased FWHM is only one amongst the other potential reasons for the decreased HFD and further investigations are needed to determine the physiological and numerical implications of this metric [35].

Not only the temporal components of muscle synergies are important for coordinated, robust control of fast locomotion: the recruitment of the appropriate muscle groups, as described by motor modules, is of critical importance too. To this extent, our results show that biarticular muscles have a speed-dependent function in both walking and running. In the weight acceptance phase, the knee extensors aid the deceleration and support of the body mass [67]. In the early swing phase, the *iliacus* and *psoas* are major hip flexors [68, 69, 70, 71, 72]. At high walking and running speeds, the biarticular RF shifts its contribution from the weight acceptance synergy (working as knee extensor) to the early swing synergy (working as hip flexor [73, 74] and as knee extensor [70, 71]). A similar behavior is evident in the relative contribution of the FL muscle to the motor modules of the weight acceptance and early swing synergies, in both walking and running. Another outcome related to motor modules was the different contribution of the GM muscle for the participants of G1 and G2. In G1 (recreational long-distance runners) the GM and GL were crucial contributors to the propulsion synergy, as found in the past [8, 9, 42, 47, 48, 49, 50]. However, in G2 (national level sprinters) the main contribution of the GM was in the weight acceptance phase: a possible indication that these muscles share little common drive when independent control is needed for secondary tasks, such as the stabilization of the ankle joint [75]. During running, the participants included in G1 adopted a different foot strike pattern than those of G2 even at similar speeds (rearfoot for G1, mid/forefoot for G2). Since rearfoot strikers need to dorsiflex the foot more than mid/forefoot strikers before touchdown [48], it is not surprising that the TA contribution to the late swing

synergy was considerable in G1 (average motor module value excluding running at 2.0 m/s: 0.57 ± 0.39), but reduced in G2 (average motor module value: 0.29 ± 0.30). Similarly, it was evident in G2 that the biarticular ST and BF were used both in the propulsion synergy and in the late swing synergy, a feature that is not visible in G1, where the ST and BF are exclusively contributing to the late swing. This confirms previous findings showing that the EMG activity of ST and BF relatively increases more during stance than during swing as the speed rises [73, 76].

In conclusion, our results show that wider, less complex muscle activation patterns are needed to cope with the challenges imposed by increased locomotion speeds. The width, complexity and modularity of muscle synergies can be regulated to ensure robust locomotion control even at very high speeds. This stands for both walking and running, with running showing generally less complex, wider motor primitives than walking.

4. Materials and methods

This study was reviewed and approved by the Ethics Committees of the Humboldt-Universität zu Berlin and Osaka University of Health and Sport Sciences. All the participants gave written informed consent for the experimental procedure, in accordance with the Declaration of Helsinki.

4.1. Experimental protocols

For the two experimental protocols we recruited 30 healthy male volunteers and divided them into two groups. The first group of 15 recreational long-distance runners (henceforth G1, height 178 ± 6 cm, body mass 71 ± 6 kg, age 33 ± 6 years, 43 ± 21 km/week running volume, personal best mark over 10 km 37.4 ± 3.2 min, means $\pm$ standard deviation) was assigned to the first experimental protocol conducted at the Humboldt-Universität zu Berlin (Germany). The second group of 15 sprint athletes (G2, height 172 ± 4 cm, body mass 65 ± 3 kg, age 21 ± 2 years, personal best mark over 100 m 10.74 ± 0.23 s) was assigned to the second experimental protocol conducted at the Osaka University of Health and Sport Sciences (Japan). Participants in G2 were younger, shorter and lighter than those of G1 ($p < 0.001$, $p = 0.009$, $p = 0.004$, respectively; independent samples, two-tailed Welch's t-test). All the participants completed a self-selected warm-up running on a treadmill, typically lasting between 3 and 5 min [49, 77]. After being instructed about the protocol, they completed a different set of measurements, depending on the protocol they were assigned to.

The experimental protocol of G1 consisted of walking (at 0.7, 1.4, and 2.0 m/s) and submaximal running (at 2.0, 3.0, and 3.5 m/s) on a single-belt treadmill (mercury, H-p-cosmos Sports & Medical GmbH, Nussdorf, Germany) equipped with a pressure plate recording the plantar pressure distribution at 120 Hz (FDM- THM-S, zebris Medical GmbH, Isny im Allgäu, Germany). The speeds were chosen as follows: walking at 1.4 m/s and running at 3.0 m/s are the commonly reported average comfortable locomotion speeds [47, 77]; 2.0 m/s is the typical walk-to-run transition speed [78, 79]; the other two speeds were chosen to extend the range of investigation.

The experimental protocol of G2 consisted of running (at 2.8, 4.2, 5.6, 6.9, 8.3, and 9.5 m/s) on a single-belt treadmill (Fully Instrumented Treadmill, Bertec co., Columbus, OH, USA) modified to reach the maximum speed of 9.5 m/s and equipped with force sensors to record the 3D ground reaction forces at 1 kHz. The highest sprinting speed was chosen to match the average pace used by the participants to run 100 m close to their personal best time.

4.2. EMG recordings

The muscle activity of the following 12 ipsilateral (right side) muscles was recorded in both groups: *gluteus maximus* (MA), *tensor fasciæ latæ* (FL), *rectus femoris* (RF), *vastus medialis* (VM), *vastus lateralis* (VL), *semitendinosus* (ST), *biceps femoris* (long head, BF), *tibialis anterior* (TA),

peroneus longus (PL), *gastrocnemius medialis* (GM), *gastrocnemius lateralis* (GL) and *soleus* (SO). The electrodes were positioned as extensively reported previously [31, 49]. After around 60 s habituation [8] in G1 or after a mild acceleration of the belt in G2 (lasting 5–10 s depending on the speed), we recorded one trial for each participant with an acquisition frequency of 2 kHz by means of a 16-channel wireless bipolar EMG system (Wave Plus wireless EMG, Cometa srl, Bareggio, Italy). For the EMG recordings, we used foam-hydrogel electrodes with snap connector (H124SG, Medtronic plc, Dublin, Ireland). The first 30 gait cycles of the recorded trial were considered for subsequent analysis [49]. Exceptions (13 out of 15 participants of G2) to this rule were applied if the participants could not sustain the imposed speed for a sufficient number of gait cycles (an event occurring only at the higher sprinting speed). All the recordings can be downloaded from the supplementary data set, which is accessible at Zenodo (https://doi.org/10.5281/zenodo.3764760).

4.3. Gait cycle parameters

The gait cycle breakdown (foot touchdown and lift-off timing) was obtained by the elaboration of the data acquired by the pressure (G1) and force (G2) plates with validated algorithms that were reported previously [77]. Other calculated gait spatiotemporal parameters were: cadence (i.e., number of steps per minute), stance and swing times and the strike index, calculated as the distance from the heel to the center of pressure at impact relative to total foot length [77]. Strike index values range from 0 to 1, denoting the most posterior and the most anterior point of the shoe, respectively [48]. Values from 0.00 to 0.33 are indication of a rearfoot strike pattern, while values from 0.34 to 1.00 represent a mid/forefoot strike pattern [77].

4.4. Muscle synergies extraction

Muscle synergies data were extracted from the recorded EMG activity through a custom script (R v3.6.3, R Core Team, 2020, R Foundation for Statistical Computing, Vienna, Austria) using the classical Gaussian NMF algorithm [8, 47, 49, 80]. The raw EMG signals were band-pass filtered within the acquisition device (cut-off frequencies 10 and 500 Hz). Then the signals were high-pass filtered, full-wave rectified and lastly low-pass filtered using a 4th order IIR Butterworth zero-phase filter with cut-off frequencies 50 Hz (high-pass) and 20 Hz (low-pass for creating the linear envelope of the signal) as previously described [8]. After subtracting the minimum, the amplitude of the EMG recordings obtained from the single trials was normalized to the maximum activation recorded for every individual muscle (i.e., every EMG channel was normalized to its maximum in every trial) [31, 49]. Each gait cycle was then time-normalized to 200 points, assigning 100 points to the stance and 100 points to the swing phase [8, 31, 48, 49]. The reason for this choice is twofold [49]. First, dividing the gait cycle into two macro-phases helps the reader understanding the temporal contribution of the different synergies, diversifying between stance and swing. Second, normalizing the duration of stance and swing to the same number of points for all participants (and for all the recorded gait cycles of each participant) makes the interpretation of the results independent of the absolute duration of the gait events. Synergies were then extracted through NMF as previously described [8, 49]. The 12 muscles listed above were considered for the analysis, (MA, FL, RF, VM, VL, ST, BF, TA, PL, GM, GL and SO). The m = 12 time-dependent muscle activity vectors were grouped in a matrix V with dimensions m × n (m rows and n columns). The dimension n represented the number of normalized time points (i.e., 200*number of gait cycles). The matrix V was factorized using NMF so that $V \approx V_R = WH$. The new matrix V_R, reconstructed multiplying the two matrices W and H, approximates the original matrix V. The motor primitives [47, 81] matrix H contained the time-dependent coefficients of the factorization with dimensions r × n, where the number of rows r represents the minimum number of synergies necessary to satisfactorily reconstruct the original set of signals V. The motor modules [47, 82]

matrix W, with dimensions m × r, contained the time-invariant muscle weightings, which describe the relative contribution of single muscles within a specific synergy (a weight was assigned to each muscle for every synergy). H and W described the synergies necessary to accomplish the required task (i.e., walking or running). The update rules for W and H are presented in Equation (Eq 1) and Equation (Eq 2).

$$\begin{cases} H_{i+1} = H_i \dfrac{W_i^T V}{W_i^T W_i H_i} & (1) \\[2mm] W_{i+1} = W_i \dfrac{V(H_{i+1})^T}{W_i H_{i+1}(H_{i+1})^T} & (2) \end{cases}$$

The quality of reconstruction was assessed by measuring the coefficient of determination R^2 between the original and the reconstructed data (V and V_R, respectively). The limit of convergence for each synergy was reached when a change in the calculated R^2 was smaller than the 0.01% in the last 20 iterations [47] meaning that, with that amount of synergies, the signal could not be reconstructed any better. This operation was first completed by setting the number of synergies to 1. Then, it was repeated by increasing the number of synergies each time, until a maximum of 9 synergies. The number 9 was chosen to be lower than the number of muscles, since extracting a number of synergies equal to the number of measured EMG activities would not reduce the dimensionality of the data. Specifically, 9 is the rounded 75% of 12, which is the number of considered muscles [31]. For each synergy, the factorization was repeated 10 times, each time creating new randomized initial matrices W and H, in order to avoid local minima [83]. The solution with the highest R^2 was then selected for each of the 9 synergies. To choose the minimum number of synergies required to represent the original signals, the curve of R^2 values versus synergies was fitted using a simple linear regression model, using all 9 synergies. The mean squared error [84] between the curve and the linear interpolation was then calculated. Afterwards, the first point in the R^2-vs.-synergies curve was removed and the error between this new curve and its new linear interpolation was calculated. The operation was repeated until only two points were left on the curve or until the mean squared error fell below 10^{-4}. This was done to search for the most linear part of the R^2-versus-synergies curve, assuming that in this section the reconstruction quality could not increase considerably when adding more synergies to the model.

4.5. Higuchi's fractal dimension of motor primitives

To assess the local complexity [85] of motor primitives, we calculated the HFD assuming that these time series exhibit self-affinity properties [9, 31, 32, 33, 52, 86, 87]. Following the procedure first described by Higuchi [32], for each motor primitive $H(t)[H(1), H(2), \dots H(n)]$, k sets of new time series must be constructed, where k is an integer interval time and $2 < k < k_{max}$:

$$H_k^{t_0} : H(t_0), H(t_0 + k), H(t_0 + 2k), \dots, H\left[t_0 + int\left(\frac{n - t_0}{k}\right)k\right] \quad (3)$$

where t_0 is the first sample at initial time. The non-Euclidean length of each curve was defined as

$$L_{t_0}(k) = \frac{1}{k} \left\{ \frac{n-1}{int\left(\frac{n-t_0}{k}\right)k} \left[\sum_{i=1}^{int\left(\frac{n-t_0}{k}\right)k} |H(t_0 + ik) - H(t_0 + (i-1)k)| \right] \right\} \quad (4)$$

and for every considered k step the length of the motor primitive was defined as the average of the k sets of lengths as

$$L(k) = \frac{1}{k} \sum_{t_0=1}^{k} L_{t_0}(k) \quad (5)$$

If $L(k) \propto k^{-HFD}$, then the curve is fractal with dimension HFD and this

should lead the plot of log($L(k)$) versus log($1/k$) to fall on a straight line with slope -HFD. The values of the HFD range from 1 (e.g., for a smooth linear time series) to 2 (e.g., for random white noise) and are independent on the amplitude of the signal, since the curve log($L(k)$) versus log($1/k$) changes intercept but not slope if the same signal is multiplied or divided [52, 87]. For each trial, the HFD of the primitives obtained by NMF was calculated separately and then averaged, so that each trial ultimately consisted of one HFD value [9]. Following suggestions from previous studies, k_{max} was chosen as the most linear part of the log-log plot, which in our data led us to choose $k_{max} = 10$ [31, 88].

4.6. Width of motor primitives

We compared motor primitives by evaluating the full width at half maximum (FWHM), a metric useful to describe the duration of activation patterns [4, 8, 31, 39]. The FWHM was calculated cycle-by-cycle after subtracting the cycle's minimum as the number of points exceeding each cycle's half maximum, and then averaged [39]. The FWHM (and just this parameter) was calculated only for the motor primitives relative to fundamental synergies. A fundamental synergy can be defined as an activation pattern whose motor primitive shows a single main peak of activation [8]. When two or more fundamental synergies are blended into one, a combined synergy appears. Combined synergies usually constitute, in our locomotion data, 10–30% of the total extracted synergies. While fundamental synergies can be compared given their similar function (i.e., motor primitives and motor modules are comparable since they serve a specific task within the step cycle), combined synergies often differ from one another making their classification impossible. Due to the lack of consensus in the literature on how to interpret them, we excluded the combined synergies from the FWHM (but not the HFD) analysis.

4.7. Functional classification of muscle synergies

The recognition of fundamental synergies was carried out by clustering similar motor primitives through NMF, using the same algorithm employed for synergy extraction with the maximum number of synergies set to the maximum factorization rank plus one. The obtained "principal shapes" (four for G1 walking, G1 running and G2 running) were then compared to the motor primitives in order to cluster similar shapes. A primitive was considered similar to one of the principal shapes if the NMF weight was equal at least to the average of all weights. Of all the primitives that satisfied this condition, we then calculated the R^2 with the relevant principal shape. If the R^2 was at least the 25% (or four times if the R^2 was negative) of the average R^2 obtained by comparing all the remaining primitives with their own principal shape, we confirmed the synergy as fundamental and classified it based on function. Primitives that were not clustered, were labelled as combined.

4.8. Statistics

To investigate the effect of locomotion speed on the factorization rank, gait parameters, HFD and FWHM of motor primitives, and motor modules we fitted the data using a generalized linear model with Gaussian error distribution. The homogeneity of variances was tested using the Levene's test. If the residuals were normally distributed, we carried out a one-way repeated measures ANOVA with type II sum of squares for the dependent variables factorization rank, cadence, stance and swing time, HFD and FWHM, the independent variable being the locomotion speed. If the normality assumptions on the residuals were not met, we used the non-parametric Kruskal-Wallis test. For the motor modules, we carried out a two-way repeated measures ANOVA with type II sum of squares, the independent variables being the speed and the muscles. If the normality assumptions on the residuals were not met, we used a robust (rank-based) ANOVA from the R package Rfit (function "raov") [89, 90]. We then performed a least significant difference *post-hoc* analysis with false discovery rate adjustment of the α level.

Otherwise, all the significance levels were set to α = 0.05 and the statistical analyses were conducted using R v3.6.3.

4.9. Data availability

In the supplementary data set accessible at Zenodo (https://doi.org/10.5281/zenodo.3764760) we made available: a) the metadata with anonymized participant information, b) the raw EMG, c) the touchdown and lift-off timings of the recorded limb, d) the filtered and time-normalized EMG, e) the muscle synergies extracted via NMF and f) the code to process the data, including the scripts to calculate the HFD of motor primitives. In total, 180 trials from 30 participants are included in the supplementary data set.

The file "metadata.dat" is available in ASCII and RData format and contains:

- Code: the participant's code
- Group: the experimental group in which the participant was involved (G1 = walking and submaximal running; G2 = submaximal and maximal running)
- Sex: the participant's sex (M or F)
- Speeds: the type of locomotion (W for walking or R for running) and speed at which the recordings were conducted in 10*[m/s]
- Age: the participant's age in years
- Height: the participant's height in [cm]
- Mass: the participant's body mass in [kg]
- PB: 100 m-personal best time (for G2).

The files containing the gait cycle breakdown are available in RData format, in the file named "CYCLE_TIMES.RData". The files are structured as data frames with as many rows as the available number of gait cycles and two columns. The first column named "touchdown" contains the touchdown incremental times in seconds. The second column named "stance" contains the duration of each stance phase of the right foot in seconds. Each trial is saved as an element of a single R list. Trials are named like "CYCLE_TIMES_P20_R_20," where the characters "CYCLE_TIMES" indicate that the trial contains the gait cycle breakdown times, the characters "P20" indicate the participant number (in this example the 20th), the character "R" indicate the locomotion type (W = walking, R = running), and the numbers "20" indicate the locomotion speed in 10*m/s (in this case the speed is 2.0 m/s). Please note that the following trials include less than 30 gait cycles (the actual number shown between parentheses): P16_R_83 (20), P16_R_95 (25), P17_R_28 (28), P17_R_83 (24), P17_R_95 (13), P18_R_95 (23), P19_R_95 (18), P20_R_28 (25), P20_R_42 (27), P20_R_95 (25), P22_R_28 (23), P23_R_28 (29), P24_R_28 (28), P24_R_42 (29), P25_R_28 (29), P25_R_95 (28), P26_R_28 (29), P26_R_95 (28), P27_R_28 (28), P27_R_42 (29), P27_R_95 (24), P28_R_28 (29), P29_R_95 (17).

The files containing the raw, filtered and the normalized EMG data are available in RData format, in the files named "RAW_EMG.RData" and "FILT_EMG.RData". The raw EMG files are structured as data frames with as many rows as the amount of recorded data points and 13 columns. The first column named "time" contains the incremental time in seconds. The remaining 12 columns contain the raw EMG data, named with muscle abbreviations that follow those reported above. Each trial is saved as an element of a single R list. Trials are named like "RAW_EMG_P03_R_30", where the characters "RAW_EMG" indicate that the trial contains raw emg data, the characters "P03" indicate the participant number (in this example the 3rd), the character "R" indicate the locomotion type (see above), and the numbers "30" indicate the locomotion speed (see above). The filtered and time-normalized emg data is named, following the same rules, like "FILT_EMG_P03_R_30".

The files containing the muscle synergies extracted from the filtered and normalized EMG data are available in RData format, in the file named "SYNS.RData". Each element of this R list represents one trial and contains the factorization rank (list element named "synsR2"), the motor

modules (list element named "W"), the motor primitives (list element named "H"), the reconstructed EMG (list element named "Vr"), the number of iterations needed by the NMF algorithm to converge (list element named "iterations"), and the reconstruction quality measured as the coefficient of determination (list element named "R2"). The motor modules and motor primitives are presented as direct output of the factorization and not in any functional order. Motor modules are data frames with 12 rows (number of recorded muscles) and a number of columns equal to the number of synergies (which might differ from trial to trial). The rows, named with muscle abbreviations that follow those reported above, contain the time-independent coefficients (motor modules M), one for each synergy and for each muscle. Motor primitives are data frames with 6000 rows and a number of columns equal to the number of synergies (which might differ from trial to trial) plus one. The rows contain the time-dependent coefficients (motor primitives P), one column for each synergy plus the time points (columns are named e.g., "time, Syn1, Syn2, Syn3", where "Syn" is the abbreviation for "synergy"). Each gait cycle contains 200 data points, 100 for the stance and 100 for the swing phase which, multiplied by the 30 recorded cycles, result in 6000 data points distributed in as many rows. This output is transposed as compared to the one discussed in the methods section to improve user readability. Trials are named like "SYNS_ P12_W_07", where the characters "SYNS" indicate that the trial contains muscle synergy data, the characters "P12" indicate the participant number (in this example the 12th), the character "W" indicate the locomotion type (see above), and the numbers "07" indicate the speed (see above). Given the nature of the NMF algorithm for the extraction of muscle synergies, the supplementary data set might show non-significant differences as compared to the one used for obtaining the results of this paper.

The files containing the HFD calculated from motor primitives are available in RData format, in the file named "HFD.RData". HFD results are presented in a list of lists containing, for each trial, 1) the HFD, and 2) the time interval k_{max} used for the calculations. HFDs are presented as one number (mean HFD of the primitives for that trial), as are the time intervals. Trials are named like "HFD_P01_R_95", where the characters "HFD" indicate that the trial contains HFD data, the characters "P01" indicate the participant number (in this example the 1st), the character "R" indicates the locomotion type (see above), and the numbers "95" indicate the speed (see above).

All the code used for the pre-processing of EMG data, the extraction of muscle synergies and the calculation of HFD is available in R format. Explanatory comments are profusely present throughout the script "muscle_synergies.R".

Declarations

Author contribution statement

A. Santuz: Conceived and designed the experiments; Performed the experiments; Analyzed and interpreted the data; Wrote the paper.

M. Ishikawa: Conceived and designed the experiments; Performed the experiments; Wrote the paper.

A. Arampatzis Conceived and designed the experiments; Wrote the paper.

A. Ekizos and K. Kijima: Performed the experiments; Wrote the paper.

Y. Kunimasa: Performed the experiments; Analyzed and interpreted the data; Wrote the paper.

Declaration of interests statement

The authors declare no conflict of interest.

Additional information

No additional information is available for this paper.

References

[1] R. Margaria, P. Cerretelli, P. Aghemo, G. Sassi, Energy cost of running, J. Appl. Physiol. 18 (1963) 367–370.

[2] G.A. Cavagna, F.P. Saibene, R. Margaria, Mechanical work in running, J. Appl. Physiol. 19 (1964) 249–256. http://www.ncbi.nlm.nih.gov/pubmed/10441084.

[3] F. Saibene, A.E. Minetti, Biomechanical and physiological aspects of legged locomotion in humans, Eur. J. Appl. Physiol. 88 (2003) 297–316.

[4] G. Cappellini, Y.P. Ivanenko, R.E. Poppele, F. Lacquaniti, Motor patterns in human walking and running, J. Neurophysiol. 95 (2006) 3426–3437.

[5] R. Margaria, Sulla fisiologia, e specialmente sul consumo energetico, della marcia e della corsa a varie velocità ed inclinazioni del terreno, Atti Dell'Accademia Naz. Dei Lincei, Rend. Della Cl. Di Sci. Fis. Mat. e Nat. 7 (1938).

[6] D.W. Morgan, P.E. Martin, G.S. Krahenbuhl, Factors affecting running economy, Sports Med. 7 (1989) 310–330. http://europepmc.org/abstract/MED/2662320.

[7] L.G.C.E. Pugh, Oxygen intake in track and treadmill running with observations on the effect of air resistance, J. Physiol. 207 (1970) 823–835.

[8] A. Santuz, A. Ekizos, N. Eckardt, A. Kibele, A. Arampatzis, Challenging human locomotion: stability and modular organisation in unsteady conditions, Sci. Rep. 8 (2018) 2740.

[9] A. Santuz, L. Brüll, A. Ekizos, A. Schroll, N. Eckardt, A. Kibele, M. Schwenk, A. Arampatzis, Neuromotor dynamics of human locomotion in challenging settings, IScience 23 (2020) 100796.

[10] N.A. Bernstein, The Co-ordination and Regulation of Movements, Pergamon Press Ltd., Oxford, 1967.

[11] E. Bizzi, F.A. Mussa-Ivaldi, S.F. Giszter, Computations underlying the execution of movement: a biological perspective, Science (80-.) 253 (1991) 287–291.

[12] S. Grillner, Biological pattern generation: the cellular and computational logic of networks in motion, Neuron 52 (2006) 751–766.

[13] T.G. Brown, The intrinsic factors in the act of progression in the mammal, Proc. R. Soc. Lond. - Ser. B Contain. Pap. a Biol. Character 84 (1911) 308–319.

[14] I.A. Rybak, K.J. Dougherty, N.A. Shevtsova, Organization of the mammalian locomotor CPG: review of computational model and circuit architectures based on genetically identified spinal interneurons, ENeuro 2 (2015) 1–21.

[15] O. Kiehn, S.J.B. Butt, Physiological, anatomical and genetic identification of CPG neurons in the developing mammalian spinal cord, Prog. Neurobiol. 70 (2003) 347–361.

[16] J.M. Cregg, R. Leiras, A. Montalant, P. Wanken, I.R. Wickersham, O. Kiehn, Brainstem neurons that command mammalian locomotor asymmetries, Nat. Neurosci. 23 (2020) 730–740.

[17] A. Santuz, O. Laflamme, B. Ross, L. Brüll, A. Arampatzis, T. Akay, Modulation of muscle synergies via supraspinal proprioceptive pathways, in: ISEK Int. Soc. Electrophysiol. Kinesiol., XXIII, 2020, p. 52. Nagoya.

[18] C.S. Sherrington, The Integrative Action of the Nervous System, first ed., Yale University Press, New Haven, CT, 1906. https://archive.org/details/integrativeacti o00sheruoft.

[19] T.G. Brown, On the nature of the fundamental activity of the nervous centres; together with an analysis of the conditioning of rhythmic activity in progression, and a theory of the evolution of function in the nervous system, J. Physiol. 48 (1914) 18–46.

[20] D.M. Wilson, The central nervous control of flight in a locust, J. Exp. Biol. 38 (1961) 471–490. http://scholar.google.com/scholar?q=related:-mDWftfrzV4J:schol ar.google.com/&hl=en&num=30&as_sdt=0,5%5Cnpapers3://publication/uu id/3E638EDB-C9F1-4B03-85B6-08B2942B3834.

[21] U. Bässler, Effects of crossing the receptor apodeme of the femoral chordotonal organ on walking, jumping and singing in locusts and grasshoppers, J. Comp. Physiol. A. 134 (1979) 173–176.

[22] D. Bucher, T. Akay, R.A. DiCaprio, A. Büschges, Interjoint coordination in the stick insect leg-control system: the role of positional signaling, J. Neurophysiol. 89 (2003) 1245–1255.

[23] D. Hess, A. Büschges, Role of proprioceptive signals from an insect femur-tibia joint in patterning motoneuronal activity of an adjacent leg joint, J. Neurophysiol. 81 (1999) 1856–1865.

[24] A. Büschges, T. Akay, J.P. Gabriel, J. Schmidt, Organizing network action for locomotion: insights from studying insect walking, Brain Res. Rev. 57 (2008) 162–171.

[25] T. Akay, B.C. Ludwar, M.L. Goritz, J. Schmitz, A. Büschges, Segment specificity of load signal processing depends on walking direction in the stick insect leg muscle control system, J. Neurosci. 27 (2007) 3285–3294.

[26] E. Bizzi, V.C.-K. Cheung, A. D'Avella, P. Saltiel, M.C. Tresch, Combining modules for movement, Brain Res. Rev. 57 (2008) 125–133.

[27] L.H. Ting, H.J. Chiel, R.D. Trumbower, J.L. Allen, J.L. McKay, M.E. Hackney, T.M. Kesar, Neuromechanical principles underlying movement modularity and their implications for rehabilitation, Neuron 86 (2015) 38–54.

[28] F. Lacquaniti, Y.P. Ivanenko, M. Zago, Patterned control of human locomotion, J. Physiol. 590 (2012) 2189–2199.

[29] M.C. Tresch, P. Saltiel, E. Bizzi, The construction of movement by the spinal cord, Nat. Neurosci. 2 (1999) 162–167.

[30] S.F. Giszter, Motor primitives-new data and future questions, Curr. Opin. Neurobiol. 33 (2015) 156–165.

[31] A. Santuz, T. Akay, W.P. Mayer, T.L. Wells, A. Schroll, A. Arampatzis, Modular organization of murine locomotor pattern in the presence and absence of sensory feedback from muscle spindles, J. Physiol. 597 (2019) 3147–3165.

[32] T. Higuchi, Approach to an irregular time series on the basis of the fractal theory, Phys. Nonlinear Phenom. 31 (1988) 277–283.

[33] B.B. Mandelbrot, Self-affine fractals and fractal dimension, Phys. Scripta 32 (1985) 257–260.

[34] L. Liehr, P. Massopust, On the mathematical validity of the Higuchi method, Phys. Nonlinear Phenom. 402 (2020) 132265.

[35] A. Santuz, T. Akay, Fractal analysis of muscle activity patterns during locomotion: pitfalls and how to avoid them, J. Neurophysiol. 124 (2020) 1083–1091.

[36] H. Kitano, Biological robustness, Nat. Rev. Genet. 5 (2004) 826–837.

[37] A.H. Meghdadi, On robustness of evolutionary fuzzy control systems, in: IEEE Annu. Meet. Fuzzy Information, 2004. Process. NAFIPS '04., 1, IEEE, 2004, pp. 254–258.

[38] G. Shinar, M. Feinberg, Structural sources of robustness in biochemical reaction networks, Science (80-.) 327 (2010) 1389–1391.

[39] G. Martino, Y.P. Ivanenko, M. Serrao, A. Ranavolo, A. D'Avella, F. Draicchio, C. Conte, C. Casali, F. Lacquaniti, Locomotor patterns in cerebellar ataxia, J. Neurophysiol. 112 (2014) 2810–2821.

[40] G. Martino, Y.P. Ivanenko, A. D'Avella, M. Serrao, A. Ranavolo, F. Draicchio, G. Cappellini, C. Casali, F. Lacquaniti, Neuromuscular adjustments of gait associated with unstable conditions, J. Neurophysiol. 114 (2015) 2867–2882.

[41] G. Cappellini, Y.P. Ivanenko, G. Martino, M.J. MacLellan, A. Sacco, D. Morelli, F. Lacquaniti, Immature spinal locomotor output in children with cerebral palsy, Front. Physiol. 7 (2016) 1–21.

[42] L. Janshen, A. Santuz, A. Ekizos, A. Arampatzis, Fuzziness of muscle synergies in patients with multiple sclerosis indicates increased robustness of motor control during walking, Sci. Rep. 10 (2020) 7249.

[43] R.L. Routson, S.A. Kautz, R.R. Neptune, Modular organization across changing task demands in healthy and poststroke gait, Phys. Rep. 2 (2014) 1–14.

[44] B. Kibushi, S. Hagio, T. Moritani, M. Kouzaki, Speed-dependent modulation of muscle activity based on muscle synergies during treadmill walking, Front. Hum. Neurosci. 12 (2018) 1–13.

[45] T.J.W. Buurke, C.J.C. Lamoth, L.H.V. van der Woude, A.R. den Otter, Synergistic structure in the speed dependent modulation of muscle activity in human walking, PloS One 11 (2016) 1–19.

[46] K. Gui, D. Zhang, Influence of locomotion speed on biomechanical subtask and muscle synergy, J. Electromyogr. Kinesiol. 30 (2016) 209–215.

[47] A. Santuz, A. Ekizos, L. Janshen, V. Baltzopoulos, A. Arampatzis, On the methodological implications of extracting muscle synergies from human locomotion, Int. J. Neural Syst. 27 (2017) 1750007.

[48] A. Santuz, A. Ekizos, L. Janshen, V. Baltzopoulos, A. Arampatzis, The influence of footwear on the modular organization of running, Front. Physiol. 8 (2017) 958.

[49] A. Santuz, A. Ekizos, L. Janshen, F. Mersmann, S. Bohm, V. Baltzopoulos, A. Arampatzis, Modular control of human movement during running: an open access data set, Front. Physiol. 9 (2018) 1509.

[50] L. Janshen, A. Santuz, A. Ekizos, A. Arampatzis, Modular control during incline and level walking in humans, J. Exp. Biol. 220 (2017) 807–813.

[51] A. Ekizos, A. Santuz, A. Schroll, A. Arampatzis, The maximum lyapunov exponent during walking and running: reliability assessment of different marker-sets, Front. Physiol. 9 (2018) 1101.

[52] S. Kesić, S.Z. Spasić, Application of Higuchi's fractal dimension from basic to clinical neurophysiology: a review, Comput. Methods Progr. Biomed. 133 (2016) 55–70.

[53] I. Mileti, A. Serra, N. Wolf, V. Munoz-Martel, A. Ekizos, E. Palermo, A. Arampatzis, A. Santuz, Muscle activation patterns are more constrained and regular in treadmill than in overground human locomotion, Front. Bioeng. Biotechnol. (2020).

[54] P.L. Gentili, The fuzziness of the molecular world and its perspectives, Molecules 23 (2018).

[55] S.H. Scott, Optimal feedback control and the neural basis of volitional motor control, Nat. Rev. Neurosci. 5 (2004) 532–545.

[56] J.C. Tuthill, E. Azim, Proprioception, Curr. Biol. 28 (2018) R194–R203.

[57] E. Todorov, M.I. Jordan, Optimal feedback control as a theory of motor coordination, Nat. Neurosci. 5 (2002) 1226–1235.

[58] R. Pryluk, Y. Kfir, H. Gelbard-Sagiv, I. Fried, R. Paz, A tradeoff in the neural code across regions and species, Cell 23 (2019) 22–27.

[59] C.R. Lee, C.T. Farley, Determinants of the center of mass trajectory in human walking and running, J. Exp. Biol. 201 (1998) 2935–2944.

[60] S.R. Hamner, S.L. Delp, Muscle contributions to fore-aft and vertical body mass center accelerations over a range of running speeds, J. Biomech. 46 (2013) 780–787.

[61] M.Q. Liu, F.C. Anderson, M.H. Schwartz, S.L. Delp, Muscle contributions to support and progression over a range of walking speeds, J. Biomech. 41 (2008) 3243–3252.

[62] S. Bohm, F. Mersmann, A. Santuz, A. Arampatzis, The force–length–velocity potential of the human soleus muscle is related to the energetic cost of running, Proc. R. Soc. B Biol. Sci. 286 (2019) 20192560.

[63] A. Arampatzis, G.-P. Brüggemann, V. Metzler, The effect of speed on leg stiffness and joint kinetics in human running, J. Biomech. 32 (1999) 1349–1353.

[64] A.G. Schache, A.K.M. Lai, N.A.T. Brown, K.M. Crossley, M.G. Pandy, Lower-limb joint mechanics during maximum acceleration sprinting, J. Exp. Biol. 222 (2019).

[65] Y.P. Ivanenko, R.E. Poppele, F. Lacquaniti, Five basic muscle activation patterns account for muscle activity during human locomotion, J. Physiol. 556 (2004) 267–282.

[66] W. Müller, A. Jung, H. Ahammer, Advantages and problems of nonlinear methods applied to analyze physiological time signals: human balance control as an example, Sci. Rep. 7 (2017) 1–11.

[67] S. Bohm, R. Marzilger, F. Mersmann, A. Santuz, A. Arampatzis, Operating length and velocity of human vastus lateralis muscle during walking and running, Sci. Rep. 8 (2018) 5066.

[68] T.W. Dorn, A.G. Schache, M.G. Pandy, Muscular strategy shift in human running: dependence of running speed on hip and ankle muscle performance, J. Exp. Biol. 215 (2012) 1944–1956.

[69] A. Higashihara, T. Ono, J. Kubota, T. Okuwaki, T. Fukubayashi, Functional differences in the activity of the hamstring muscles with increasing running speed, J. Sports Sci. 28 (2010) 1085–1092.

[70] T.F. Novacheck, The biomechanics of running, Gait Posture 7 (1998) 77–95. http://www.ncbi.nlm.nih.gov/pubmed/10200378.

[71] A.G. Schache, T.W. Dorn, P.D. Blanch, N.A.T. Brown, M.G. Pandy, Mechanics of the human hamstring muscles during sprinting, Med. Sci. Sports Exerc. 44 (2012) 647–658.

[72] R.A. Mann, G.T. Moran, S.E. Dougherty, Comparative electromyography of the lower extremity in jogging, running, and sprinting, Am. J. Sports Med. 14 (1986) 501–510. http://www.ncbi.nlm.nih.gov/pubmed/3799879.

[73] H. Kyröläinen, J. Avela, P.V. Komi, Changes in muscle activity with increasing running speed, J. Sports Sci. 23 (2005) 1101–1109.

[74] A. Mero, P.V. Komi, Electromyographic activity in sprinting at speeds ranging from sub-maximal to supra-maximal, Med. Sci. Sports Exerc. 19 (1987) 266–274. http://www.ncbi.nlm.nih.gov/pubmed/3600241.

[75] F. Hug, A. Del Vecchio, S. Avrillon, D. Farina, K. Tucker, Muscles from the same muscle group can be independently controlled by the central nervous system during a synergistic action, in: ISEK Int. Soc. Electrophysiol. Kinesiol., XXIII, 2020, pp. 52–53.

[76] A.G. Schache, T.W. Dorn, T.V. Wrigley, N.A.T. Brown, M.G. Pandy, Stretch and activation of the human biarticular hamstrings across a range of running speeds, Eur. J. Appl. Physiol. 113 (2013) 2813–2828.

[77] A. Santuz, A. Ekizos, A. Arampatzis, A pressure plate-based method for the automatic assessment of foot strike patterns during running, Ann. Biomed. Eng. 44 (2016) 1646–1655.

[78] A. Lai, G.A. Lichtwark, A.G. Schache, Y.-C. Lin, N.A.T. Brown, M.G. Pandy, In vivo behavior of the human soleus muscle with increasing walking and running speeds, J. Appl. Physiol. 118 (2015) 1266–1275.

[79] A. Hreljac, Preferred and energetically optimal gait transition speeds in human locomotion, Med. Sci. Sports Exerc. 25 (1993) 1158–1162.

[80] D.D. Lee, H.S. Seung, Learning the parts of objects by non-negative matrix factorization, Nature 401 (1999) 788–791.

[81] N. Dominici, Y.P. Ivanenko, G. Cappellini, A. D'Avella, V. Mondi, M. Cicchese, A. Fabiano, T. Silei, A. Di Paolo, C. Giannini, R.E. Poppele, F. Lacquaniti, Locomotor primitives in newborn babies and their development, Science (80-.) 334 (2011) 997–999.

[82] L. Gizzi, J.F. Nielsen, F. Felici, Y.P. Ivanenko, D. Farina, Impulses of activation but not motor modules are preserved in the locomotion of subacute stroke patients, J. Neurophysiol. 106 (2011) 202–210.

[83] A. D'Avella, E. Bizzi, Shared and specific muscle synergies in natural motor behaviors, Proc. Natl. Acad. Sci. U. S. A. 102 (2005) 3076–3081.

[84] V.C.-K. Cheung, A. D'Avella, M.C. Tresch, E. Bizzi, Central and sensory contributions to the activation and organization of muscle synergies during natural motor behaviors, J. Neurosci. 25 (2005) 6419–6434.

[85] T. Gneiting, M. Schlather, Stochastic models that separate fractal dimension and the hurst effect, SIAM Rev. 46 (2004) 269–282.

[86] J. Theiler, Estimating the fractal dimension of chaotic time series, Linc. Lab. J. 3 (1990) 63–86.

[87] F.M. Smits, C. Porcaro, C. Cottone, A. Cancelli, P.M. Rossini, F. Tecchio, Electroencephalographic fractal dimension in healthy ageing and alzheimer's disease, PloS One 11 (2016), e0149587.

[88] T. Gneiting, H. Ševčíková, D.B. Percival, Estimators of fractal dimension: assessing the roughness of time series and spatial data, Stat. Sci. 27 (2012) 247–277.

[89] J.D. Kloke, J.W. McKean, Rfit: rank-based estimation for linear models, R J. 4 (2012) 57–64.

[90] J.W. McKean, J.D. Kloke, Efficient and adaptive rank-based fits for linear models with skew-normal errors, J. Stat. Distrib. Appl. (2014) 1–18.